Scale Adaptive Filtering Derived from the Laplace Equation*

Michael Felsberg and Gerald Sommer
Christian-Albrechts-University of Kiel
Institute of Computer Science and Applied Mathematics
Cognitive Systems
Preußerstraße 1-9, 24105 Kiel, Germany
Tel: +49 431 560433, Fax: +49 431 560481
{mfe, gs}@ks.informatik.uni-kiel.de

August 15, 2001

Abstract

In this paper, we present a new approach to scale-space which is derived from the 3D Laplace equation instead of the heat equation. The resulting lowpass and bandpass filters are discussed and they are related to the monogenic signal. As an application, we present a scale adaptive filtering which is used for denoising images. The adaptivity is based on the local energy of spherical quadrature filters and can also be used for sparse representation of images.
Keywords: scale-space, quadrature filters, adaptive filters, denoising

*This work has been supported by German National Merit Foundation and by DFG Graduiertenkolleg No. 357 (M. Felsberg) and by DFG Grant So-320-2-2 (G. Sommer).

1 Introduction

In this paper, we present a new approach to scale-space. In the classical case, the heat equation leads to a homogeneous linear scale-space which is based on convolutions with Gaussian lowpass filters [11]. This method has been extended into several directions, in order to obtain more capable methods for low level vision. Perona and Malik introduce a diffusion constant which varies in the spatial domain controlling the grade of smoothing [12]. In his approach, Weickert substitutes the scalar product in the controlling term by the outer product yielding a method for anisotropic diffusion [15]. Sochen et. al. chose a more general point of view by considering the image intensity as a manifold [13] where the metric tensor controls the diffusion. This list is far from being complete, but what is important in this context is that all mentioned approaches have three things in common. At first, they are all based on the heat equation which can be seen as a heuristic choice from a physical model. In [16] however, several approaches for deriving the Gaussian scale-space as the unique solution of some basic axioms are presented. From our point of view, there is at least one PDE besides the diffusion equation that also generates a linear scale-space[1]. Second, all approaches try to control the diffusion by some information obtained from the image which are mostly related to partial derivatives and a measure for edges. Therefore, structures with even and odd symmetries are not weighted in the same way. Thirdly, all mentioned diffusions have theoretically infinite duration which means that the diffusion has to be stopped at a specific time. The stopping of the diffusion process is crucial for the result.

Our new method differs with respect to all three aspects from the classical ones. At first, it is based on the 3D Laplace equation which yields besides a smoothing kernel the monogenic signal, a 2D generalization of the analytic signal [6]. Extending the properties of the analytic signal to 2D, the monogenic signal is well suited for estimating the local energy of a structure independently if it has an even or odd symmetry. Hence, if the smoothing is controlled by the energy, it is independent of the local symmetry. The energy of a local structure differs with the considered scale and in general it has several local maxima. These local maxima correspond to the partial local structures which form the whole considered structure. Our approach does not control the smoothing process itself but builds up a linear scale-space and applies an appropriate post-processing. Depending on the application, a coarsest scale and a minimal local energy are chosen, which determine an appropriate 2D surface in the 3D scale-space.

[1] Our new approach fulfills all axioms of Iijima [16] (see section 3) which means that there must be an error in the proof of Iijima.

2 Theory

In this paper, images are considered as 2D real signals $f(x, y)$, whereas the scale-space is a 3D function defined over the spatial coordinates x and y and the scale parameter s. The commonly used signal model of scale-space is a stack of images, or from the physical point of view, a heat distribution at a specific time. Our model is quite different and it is motivated by two points of view. On the one hand, 1D signal processing and especially the Hilbert transform are closely related to complex analysis and holomorphic functions. On the other hand, holomorphic functions can be identified with *harmonic vector fields*, i.e., zero-divergence gradient fields. Indeed, the Hilbert transform emerges from postulating such a field in the positive half-plane $y > 0$ and by considering the relation between the components of the field on the real line [7]. Motivated by this fact, we introduce the following *signal model* (see Fig. 1). In the 3D space (x, y, s), the signal is embed-

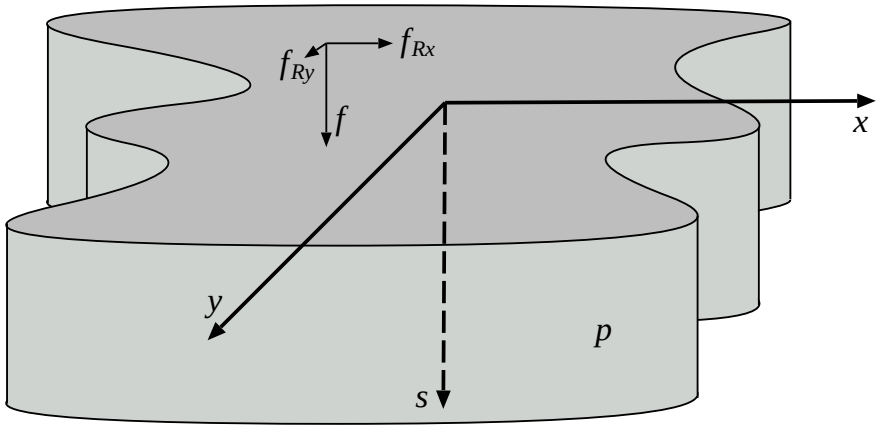

Figure 1: Signal model for 2D signals, the scale-space, and the generalized analytic signal. The signal f is given by the s-derivative of the harmonic potential p. The other two derivatives ($f_{Rx} = h_x * f$ and $f_{Ry} = h_y * f$) are the generalized Hilbert transforms of f

ded as the s-component of a 3D zero-divergence gradient field in the plane $s = 0$. For $s > 0$ the s-component is given by smoothed versions of the original image, so that the s-component corresponds to the classical scale-space. For $s = 0$ the other two components turn out to be the 2D equivalent of the Hilbert transform [7] and for $s > 0$ they are the generalized Hilbert transforms of the smoothed image. Hence, the most fundamental function in this embedding is the underlying *harmonic potential* p, i.e., p fulfills the Laplace-equation (see below). Due to the embedding, the Fourier transform is always performed wrt. x and y only, with the

corresponding frequencies u and v. Accordingly, convolutions are also performed wrt. x and y only.

As already mentioned in the introduction and according to the signal model, we derive the non-Gaussian linear scale-space from the 3D Laplace equation ($\Delta_3 = \partial_x^2 + \partial_y^2 + \partial_s^2$ indicating the 3D Laplace operator)

$$\Delta_3 p(x, y, s) = 0 \ . \tag{1}$$

The fundamental solution is given by $p(x, y, s) = c(x^2+y^2+s^2)^{-1/2}$ (the Newton potential) [3] where c is a constant that we choose to be $-(2\pi)^{-1}$. Since derivative operators commute, the partial derivatives of $p(x, y, s)$ are also solutions of (1) (comparable to the fact that the real part and the imaginary part of a holomorphic function are harmonic functions). Therefore, we obtain the (conjugated) Poisson kernels as further solutions [14]

$$g(x, y, s) = \frac{\partial}{\partial s}\frac{-1}{2\pi(x^2+y^2+s^2)^{1/2}} = \frac{s}{2\pi(x^2+y^2+s^2)^{3/2}} \tag{2}$$

$$h_x(x, y, s) = \frac{\partial}{\partial x}\frac{-1}{2\pi(x^2+y^2+s^2)^{1/2}} = \frac{x}{2\pi(x^2+y^2+s^2)^{3/2}} \tag{3}$$

$$h_y(x, y, s) = \frac{\partial}{\partial y}\frac{-1}{2\pi(x^2+y^2+s^2)^{1/2}} = \frac{y}{2\pi(x^2+y^2+s^2)^{3/2}} \ . \tag{4}$$

By taking the limit $s \to 0$, g is the delta-impulse $\delta_0(x)\delta_0(y)$ (representing the identity operator) and $(h_x, h_y)^T$ are the kernels of the Riesz transforms, so that $(g, h_x, h_y)^T * f$ is the monogenic signal of the real signal f [6]. Quite more interesting in this context is the fact that for $s > 0$ $(g, h_x, h_y)^T * f$ is the monogenic signal of the lowpass filtered signal $g * f$. This follows immediately from the transfer functions corresponding to (2–4) ($q = \sqrt{u^2+v^2}$):

$$G(u, v, s) = \exp(-2\pi q s) \tag{5}$$

$$H_x(u, v, s) = -i\, u/q\, \exp(-2\pi q s) \tag{6}$$

$$H_y(u, v, s) = -i\, v/q\, \exp(-2\pi q s) \ . \tag{7}$$

The derivation of the transfer functions can be found in the appendix. Besides, the Laplace equation (1) can also solved by separating (x, y) and s giving two factors: one is the kernel of the 2D Fourier transform $\exp(-i2\pi(ux + vy))$ and the other one is $G(u, v, s)$ see [8]. Hence, instead of forming the scalar valued scale-space by $g(x, y, s) * f(x, y)$, we build a *vector field* $\mathbf{f}$:

$$\mathbf{f}(x, y, s) = (\ g(x, y, s)\ h_x(x, y, s)\ h_y(x, y, s)\ )^T * f(x, y) \tag{8}$$

which is not only a family of monogenic signals (for different values of s) but also a solenoidal and irrotational field (which means that divergence and rotation are both zero), or, in terms of Geometric Algebra, a monogenic function [5] (monogenic: nD generalization of holomorphic).

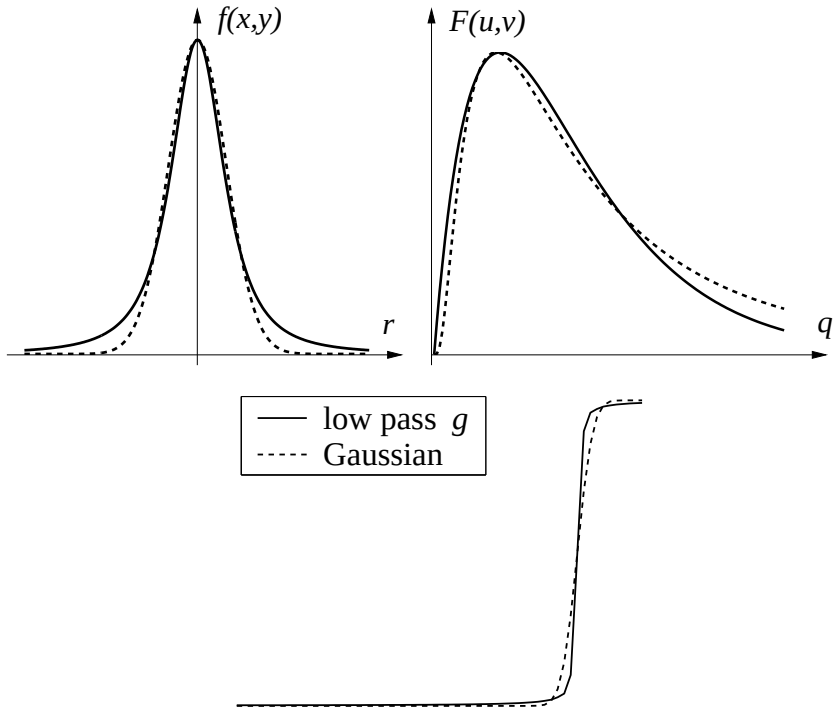

Figure 2: Upper left: impulse response of lowpass filter g (solid line) and impulse response of Gaussian lowpass filter (dotted line). Upper right: transfer function of the difference of two lowpass filters for different scales s and s' (solid line) and transfer function of the lognormal bandpass (dotted line). Bottom: lowpass filters applied to a step edge

3 A New Linear Scale-Space

Now, getting from the mathematical background to interpretation, we firstly consider the shape of the derived lowpass filter g and the transfer function of the difference of two lowpass filters with different values of s, see Fig. 2. All four filters are isotropic and hence, they are plotted wrt. to the radial coordinate $r = \sqrt{x^2 + y^2}$ and the radial frequency q, respectively. The impulse response of g has a sharper peak than the one of the Gaussian lowpass. On the other hand, it decreases slower with increasing r. Accordingly, steps in the image are changed according to Fig. 2 (right). While the curvature is smoother in the case of the filter g, the slope of the edge is more reduced by the Gaussian filter. Adopting the idea of the Laplacian pyramid [4], we use the difference of two lowpass filters to obtain a bandpass filter. It has a zero DC component and is similar to the lognormal bandpass, but it has a singularity in the first derivative for $q = 0$[2]. Hence,

[2]Note that this is not valid for the transfer functions (6) and (7).

low frequencies are not damped as much as in the lognormal case, but for high frequencies, the transfer function G decreases faster.

Considering the uncertainty relation, the lowpass filter g is slightly worse than the Gaussian lowpass (factor $\sqrt{1.5}$, see appendix) which means that the localization in phase space is not far from being optimal. In contrast to the lognormal bandpass filter, the spatial representation of the new bandpass filter is given analytically, so that it can be constructed in the spatial domain more easily. What is even more important, is that the linear combination of lowpass filtered monogenic signals is again a monogenic signal. Therefore, the difference of two of these signals is a *spherical quadrature filter* (see also [5]). The last property of the new lowpass / bandpass filters which is important in the following, is the energy. The DC-component of the lowpass filter is one by definition (5). The bandpass filters for a multi-band decomposition are constructed according to

$$B_k(u,v) = \exp(-2\pi\sqrt{u^2+v^2}s_0\lambda^k) - \exp(-2\pi\sqrt{u^2+v^2}s_0\lambda^{k-1}) \qquad (9)$$

where $\lambda \in (0;1)$ indicates the relative bandwidth, s_0 indicates the coarsest scale, and $k \in \mathbb{N}$ indicates the octave. The maximal energy of the bandpass filter is independent of k.

What is left to show is that the Poisson kernel (2) really establishes a linear scale-space. According to [16], Iijima defines in [9] a linear scale-space by five axioms:

1. The generating kernel of a linear scale-space is *linear*.
2. The kernel is *shift invariant*.
3. The kernel fulfills the *semigroup property*.
4. The kernel is *scale invariant*.
5. The kernel *preserves positivity*.

Iijima showed that the Gaussian kernel is the *unique solution* of the previous axioms. Nevertheless, one can show that the Poisson kernel *also* fulfills all five axioms:

1. The Poisson kernel is a linear, shift-invariant operator.
2. See above.
3. This axiom is easily verified in the Frequency domain:

$$\exp(-2\pi q s_1)\exp(-2\pi q s_2) = \exp(-2\pi q(s_1+s_2)) \ ,$$

hence $g(x,y,s_1) * g(x,y,s_2) = g(x,y,s_1+s_2)$.

4. The scale invariance is checked in the spatial domain ($\lambda \in \mathbb{R}^+$):

$$\begin{aligned} g(\lambda x, \lambda y, s) &= \frac{s}{2\pi(\lambda^2(x^2+y^2)+s^2)^{\frac{3}{2}}} \\ &= \frac{\frac{s}{\lambda}}{2\pi\left(x^2+y^2+\left(\frac{s}{\lambda}\right)^2\right)^{\frac{3}{2}}}\ \frac{1}{\lambda^2} \\ &= g\left(x, y, \frac{s}{\lambda}\right)\ \frac{1}{\lambda^2}\ , \end{aligned}$$

   where λ^{-2} is the Jacobian.

5. The Poisson kernel is positivity preserving since it is positive for all $(x, y)^T \in \mathbb{R}^2$.

Both scale-space approaches, the Gaussian scale-space and the Poisson scale-space, can be compared by means of two mpeg videos which are provided together with this paper.

4 Scale Adaptive Filters

The described scale-space approach can be used to denoise images or to reduce the number of features in an image (to *sparsify* it). Our algorithm behaves as follows: the scale-space is calculated up to a maximal smoothing s_M which is sufficient to remove nearly all the noise. For each scale, the monogenic signal is calculated and an index function is defined by the finest scale with a local maximum of the local magnitude

$$\text{index}(x,y) = \begin{cases} s_m & \text{if } \exists \epsilon > 0 : |f_M(x,y,s_m)| \geq |f_M(x,y,s)|\ \forall s < s_m + \epsilon \\ & \quad \wedge \quad s_m < s_M \quad \wedge \quad |f_M(x,y,s_m)|^2 \geq E_T \\ s_M & \text{else} \end{cases} \tag{10}$$

where the coarsest scale s_M is chosen if the maximal energy is lower than a threshold E_T. Using this index function, a denoised image is constructed, where at each position the lowpass is chosen by the index. The algorithm is motivated by the fact that the response of the monogenic signal shows local maxima when it is applied in the 'correct' scale, where in general we have more than one maximum. Since it is not reasonable to consider the image on arbitrary coarse scales (e.g. averaging of one quarter of the image), the range of scale is reduced and we mostly have only one maximum, see Fig. 3. The threshold of the energy at the maximum

suppresses weak textures by setting the index function to maximal smoothing. Additionally, we apply median filters to the index functions, in order to denoise the latter. It is not reasonable to have an arbitrarily changing scale index since the scale is depending on the local neighborhood.

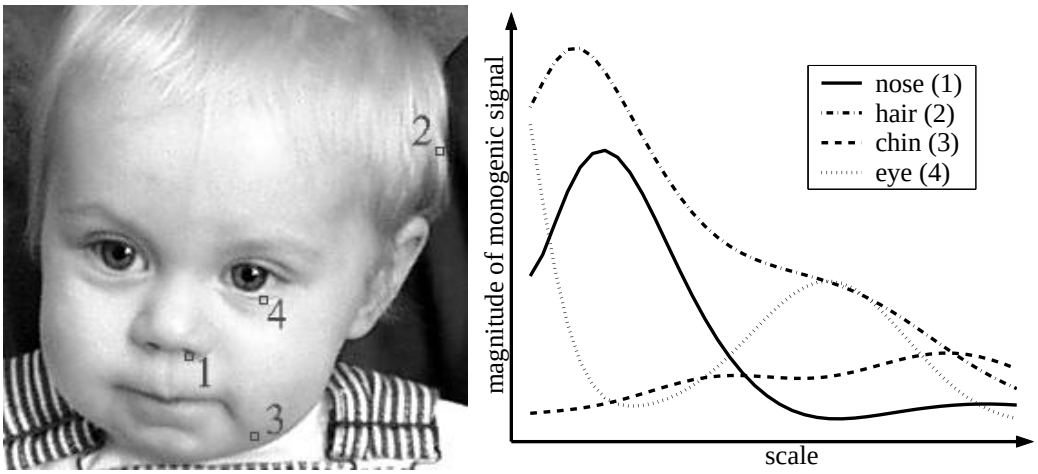

Figure 3: Test image (left). The energy of the monogenic signal at four positions (indicated in the left image) for varying scale can be found in the plot on the right

In our first experiment, we applied the algorithm to the test images in Fig. 3 and Fig. 4. The images were both processed with the same threshold and the same maximal scale. In both cases, a 3x3 median filter was applied to the scale index obtained from (10). The dark shadows at the top and left border of the smoothed house-image are artifacts resulting from performing the convolutions in the frequency domain. Obviously, textures with low energy are removed while edges and other structures with high energy are preserved. If a structure is preserved or not depends on the choice of the parameter E_T. In the case of noisy images, this energy threshold can be estimated according to a Rayleigh distribution (see [10]).

In our second experiment, we added Gaussian noise to the image in Fig. 3 (see Fig. 5, left) and applied the standard method of isotropic Gaussian diffusion to it. The result can be found in the middle image in Fig. 5. The typical behavior of Gaussian diffusion can be seen well: near the edges the noise is still present. Our approach results in the image on the right in the same figure. Except for some singular points the noise has been removed completely. The energy threshold was chosen by the method mentioned in the previous paragraph. In contrast to the diffusion algorithm, our method tends to over-smooth slightly those region boundaries where the energy of the edge is lower than the energy of the noise (see upper left corner).

The algorithm can also be used to sparsify images. Instead of constructing

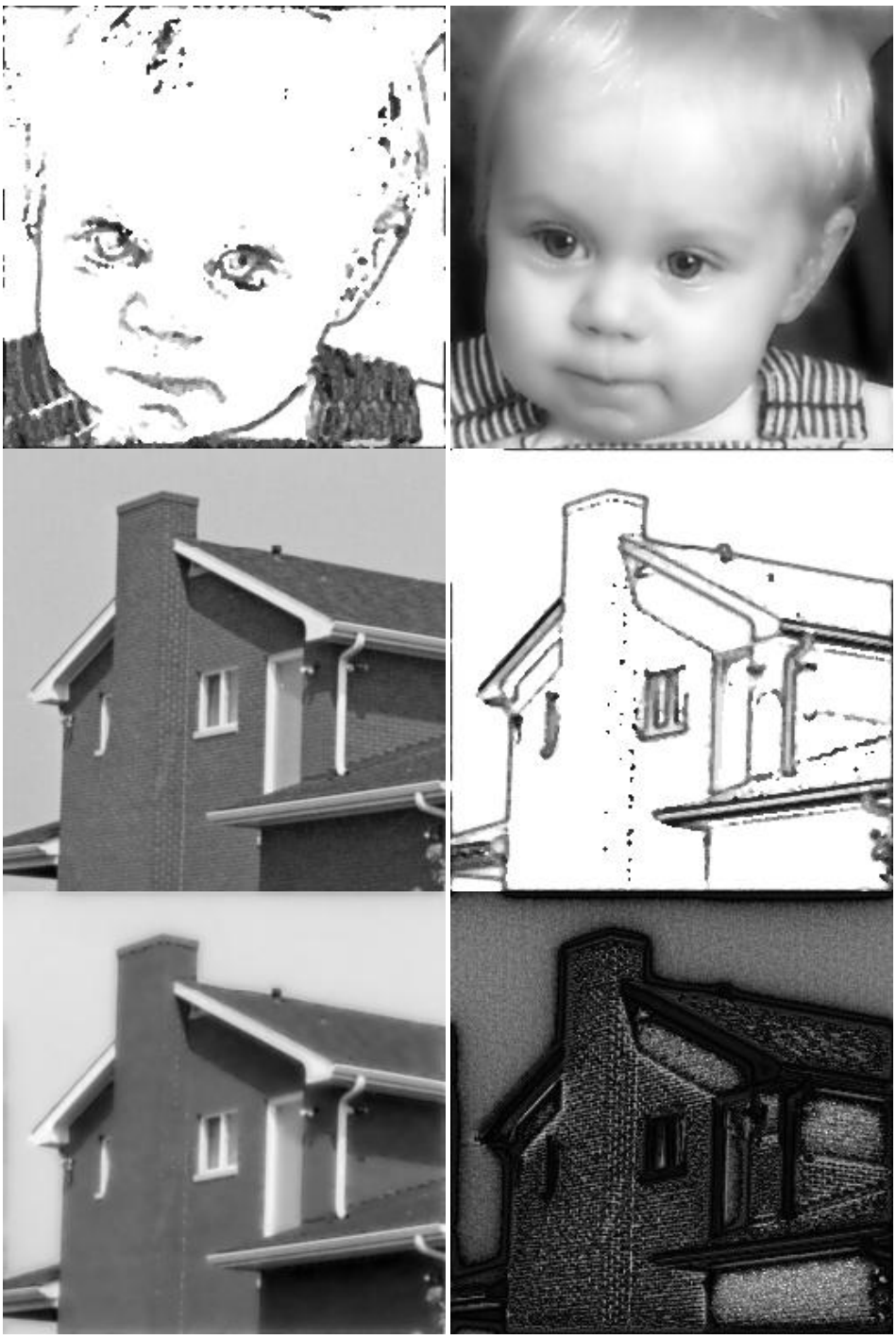

Figure 4: Upper row, left to right: scale index for first test image and smoothed image. Center row, left to right: second test image and corresponding scale index. Bottom row: smoothed image and relative difference between original and smoothed version.

Figure 5: Test image with noise (left), variance: $6e+3$. Isotropic diffusion (parameters: contrast $\lambda = 3$, noise scale $\sigma = 2$, time step $\Delta t = 0.2$, and 50 iterations) yields the result in the middle, variance: $4.5e+3$. The image on the right shows the result of our approach, variance: $3.5e+3$

the denoised image from lowpass filtered versions using the scale index, the filter response of the monogenic signal is kept for local maxima of the energy only. That means that for the 'else' case in (10) the result is set to zero (nothing is stored). The amount of the remaining information can be estimated by the dark areas in the index images in Fig. 4. The representation which is obtained includes information of the monogenic signal only at positions with high local energy at an appropriate scale.

5 Conclusion

We have presented a new approach to scale-space which is not based on the heat equation but on the 3D Laplace equation. We have shown that our approach fulfills the axioms of Iijima and hence, the Poisson kernel builds up a linear scale-space in the strong sense. The resulting lowpass and bandpass filters have been shown to work properly and a relation to spherical quadrature filters and the monogenic signal has been established. Using the energy of the monogenic signal for different scales, a scale adaptive denoising algorithm has been presented which can also be adopted for a sparse representation of features. The results are comparable to those of isotropic Gaussian diffusion. The denoising based on the Laplace equation shows less noise in the neighborhood of edges, but low-energy edges are not preserved as well as in the Gaussian case. Though it is by definition an isotropic method, the new approach can easily be extended to anisotropic denoising by introducing a 2×2 scaling matrix instead of the real scale parameter s. The behavior for low-energy edges is supposed to be better in that case.

A Appendix

A.1 Fourier Transform of the Poisson Kernel

$$\mathcal{F}_2\left\{\frac{s}{2\pi(x^2+y^2+s^2)^{3/2}}\right\}(u,v) = \exp(-2\pi qs)$$

for $s > 0$.
According to the table of Hankel transforms in [1],

$$\mathcal{F}_2\{(1+r^2)^{-3/2}\}(u,v) = 2\pi\exp(-2\pi q) \ .$$

Substituting $r' = sr$, $s > 0$ and applying the affine theorem yields

$$\mathcal{F}_2\{s^3(s^2+r'^2)^{-3/2}\}(u,v) = s^2 2\pi\exp(-2\pi qs) \ .$$

By setting $r' = \sqrt{x^2+y^2}$ and multiplying with $(s^2 2\pi)^{-1}$ the Fourier transform of the Poisson kernel is obtained.

A.2 Fourier Transform of the Conjugate Poisson Kernel

$$\mathcal{F}_2\left\{\frac{x}{2\pi(x^2+y^2+s^2)^{3/2}}\right\}(u,v) = -\frac{iu}{q}\exp(-2\pi qs)$$

for $s > 0$.
According to the table of Hankel transforms in [1],

$$\mathcal{F}_2\{(1+r^2)^{-1/2}\}(u,v) = q^{-1}\exp(-2\pi q)$$

and by substituting $r' = sr$ ($s > 0$)

$$\mathcal{F}_2\{s(s^2+r'^2)^{-1/2}\}(u,v) = s^2(qs)^{-1}\exp(-2\pi qs) \ .$$

Hence,

$$\mathcal{F}_2\{(s^2+x^2+y^2)^{-1/2}\}(u,v) = q^{-1}\exp(-2\pi qs) \ .$$

Applying the derivative theorem yields

$$\mathcal{F}_2\{-x(s^2+x^2+y^2)^{-3/2}\}(u,v) = i2\pi u\, q^{-1}\exp(-2\pi qs)$$

and by multiplying with $-\frac{1}{2\pi}$ the Fourier transform of the first conjugate Poisson kernel is obtained.

$$\mathcal{F}_2\left\{\frac{y}{2\pi(x^2+y^2+s^2)^{3/2}}\right\}(u,v) = -\frac{iv}{q}\exp(-2\pi qs)$$

is derived accordingly.

A.3 Uncertainty of the Poisson Kernel

The spread in the spatial domain reads

$$\begin{aligned}
\Delta\mathbf{x} = \sqrt{\sigma_{\mathbf{x}}^2} &= \left(\frac{\iint (x^2+y^2) g(x,y,s)^2 \, dx \, dy}{\iint g(x,y,s)^2 \, dx \, dy} \right)^{1/2} \\
&= \left(\frac{\iint (x^2+y^2) \frac{s^2}{4\pi^2 (x^2+y^2+s^2)^3} \, dx \, dy}{\iint \frac{s^2}{4\pi^2 (x^2+y^2+s^2)^3} \, dx \, dy} \right)^{1/2} \\
&= \left(\frac{\iint \frac{x^2+y^2}{(x^2+y^2+s^2)^3} \, dx \, dy}{\iint \frac{1}{(x^2+y^2+s^2)^3} \, dx \, dy} \right)^{1/2} \\
&\quad \text{change to polar coordinates } r = \sqrt{x^2+y^2}\text{:} \\
&= \left(\frac{2\pi \int_0^\infty \frac{r^3}{(r^2+s^2)^3} \, dr}{2\pi \int_0^\infty \frac{r}{(r^2+s^2)^3} \, dr} \right)^{1/2} = \left(\frac{\frac{1}{2s^2} - \frac{s^2}{4s^4}}{\frac{1}{4s^4}} \right)^{1/2} = s
\end{aligned}$$

where the integrals are evaluated according to [2] 19.5.1.3 integral 63 and 71. The spread in the frequency domain is obtained as

$$\begin{aligned}
\Delta\mathbf{u} = \sqrt{\sigma_{\mathbf{u}}^2} &= \left(\frac{\iint (u^2+v^2) G(u,v,s)^2 \, du \, dv}{\iint G(u,v,s)^2 \, du \, dv} \right)^{1/2} \\
&= \left(\frac{\iint (u^2+v^2) \exp(-4\pi\sqrt{u^2+v^2} s) \, du \, dv}{\iint \exp(-4\pi\sqrt{u^2+v^2} s) \, du \, dv} \right)^{1/2} \\
&\quad \text{change to polar coordinates } q = \sqrt{u^2+v^2}\text{:} \\
&= \left(\frac{2\pi \int_0^\infty q^3 \exp(-4\pi q s) \, dq}{2\pi \int_0^\infty q \exp(-4\pi q s) \, dq} \right)^{1/2} = \left(\frac{\frac{6}{(4\pi s)^4}}{\frac{1}{(4\pi s)^2}} \right)^{1/2} = \frac{\sqrt{6}}{4\pi s}
\end{aligned}$$

where the integrals are evaluated according to [2] 19.6.1 integral 1. Hence

$$(\Delta\mathbf{x})(\Delta\mathbf{u}) = \frac{\sqrt{6}}{4\pi}$$

which means that the uncertainty is slightly worse than for the 2D Gaussian kernel (factor $\sqrt{1.5}$).

References

[1] BRACEWELL, R. N. *Two-Dimensional Imaging*. Prentice Hall Signal Processing Series. Prentice Hall, Englewood Cliffs, 1995.

[2] BRONSTEIN, I., SEMENDJAJEW, K., MUSIOL, G., AND MÜHLIG, H. *Taschenbuch der Mathematik*. Verlag Harri Deutsch, Frankfurt, 1993.

[3] BURG, K., HAF, H., AND WILLE, F. *Höhere Mathematik für Ingenieure, Band IV Vektoranalysis und Funktionentheorie*. Teubner Stuttgart, 1994.

[4] BURT, P. J., AND ADELSON, E. H. The Laplacian pyramid as a compact image code. *IEEE Trans. Communications 31*, 4 (1983), 532–540.

[5] FELSBERG, M., AND SOMMER, G. The multidimensional isotropic generalization of quadrature filters in geometric algebra. In *Proc. Int. Workshop on Algebraic Frames for the Perception-Action Cycle, Kiel* (2000), G. Sommer and Y. Zeevi, Eds., vol. 1888 of *Lecture Notes in Computer Science*, Springer-Verlag, Heidelberg, pp. 175–185.

[6] FELSBERG, M., AND SOMMER, G. A new extension of linear signal processing for estimating local properties and detecting features. In *22. DAGM Symposium Mustererkennung, Kiel* (2000), G. Sommer, Ed., Springer-Verlag, Heidelberg, pp. 195–202.

[7] FELSBERG, M., AND SOMMER, G. The monogenic signal. Tech. Rep. 2016, Institute of Computer Science and Applied Mathematics, Christian-Albrechts-University of Kiel, Germany, May 2001.

[8] FELSBERG, M., AND SOMMER, G. The structure multivector. In *Applied Geometrical Algebras in Computer Science and Engineering* (2001), Birkhäuser. to be published.

[9] IIJIMA, T. Basic theory of pattern observation. In *Papers of Technical Group on Automata and Automatic Control, IECE, Japan* (December 1959).

[10] KOVESI, P. Image features from phase information. *Videre: Journal of Computer Vision Research 1*, 3 (1999).

[11] LINDEBERG, T. *Scale-Space Theory in Computer Vision*. The Kluwer International Series in Engineering and Computer Science. Kluwer Academic Publishers, Boston, 1994.

[12] PERONA, P., AND MALIK, J. Scale-space and edge detection using anisotropic diffusion. *IEEE Trans. Pattern Analysis and Machine Intelligence 12*, 7 (1990), 629–639.

[13] SOCHEN, N., KIMMEL, R., AND MALLADI, R. A geometrical framework for low level vision. *IEEE Trans. on Image Processing, Special Issue on PDE based Image Processing 7*, 3 (1998), 310–318.

[14] STEIN, E. M. *Harmonic Analysis*. Princeton University Press, New Jersey, 1993.

[15] WEICKERT, J. *Anisotropic Diffusion in Image Processing*. PhD thesis, Faculty of Mathematics, University of Kaiserslautern, 1996.

[16] WEICKERT, J., ISHIKAWA, S., AND IMIYA, A. Scale-space has first been proposed in Japan. *Mathematical Imaging and Vision 10* (1999), 237–252.